Numerical analysis of the impact on infiltration on cut natural clay slopes

PAPER • **OPEN ACCESS**

Numerical analysis of the impact on infiltration on cut natural clay slopes

To cite this article: K. Muratova *et al* 2025 *IOP Conf. Ser.: Earth Environ. Sci.* **1523** 012033

IOP Conf. Series: Earth and Environmental Science **1523** (2025) 012033 doi:10.1088/1755-1315/1523/1/012033

Numerical analysis of the impact on infiltration on cut natural clay slopes

K. Muratova[1*], A. Abed[1] and M. Karstunen[1]

[1] Department of Architecture and Civil Engineering, Chalmers University of Technology, Gothenburg, Sweden

[*]E-mail: kseniia.muratova@chalmers.se

Abstract. This study presents a numerical analysis of a cut sensitive clay slope subjected to climate-induced hydrological loading. To accurately capture the coupled hydro-mechanical behaviour, simulations were performed using the FEniCS-Geo finite element framework, which solves the governing mechanical and water mass balance. The Creep-SClay1S constitutive model was employed to represent the behaviour of sensitive clay, as it accounts for key features such as anisotropy, destructuration, rate dependency as well as Lode angle. Careful attention was paid to initializing the slope with realistic in-situ stress and pore pressure conditions to ensure meaningful interpretation of the results. A sensitivity analysis was carried out for varying rainfall intensities, enabling the evaluation of how climate-related changes in infiltration affect stress redistribution and the evolution of deformation within the slope.

1. Introduction

Over the decades, landslides have remained a persistent threat to infrastructure and human safety, particularly in regions characterized by sensitive clay, such as parts of Sweden, Norway, and Canada. With the increasing impact of climate change, including more frequent and intense rainfall events, the need to better understand the processes governing slope behaviour has become more urgent (Gariano and Guzzetti [13]).

In particular, the interaction between the hydrological loading and the mechanical response in natural clays remains a key research challenge. Of special importance is the role of unloading, caused by erosion or excavation, which can substantially alter the stress field and initial state and accelerate the failure of the slope. Furthermore, variations in the rainfall infiltration can significantly affect the pore water pressure distributions, further influencing deformation patterns and slope stability (Boyle et al. [14]). Change in pore pressure leads to decrease in the effective stresses in the soil, which leads to decreased mobilised shear strength. Depending on the stresses, soil response upon wetting is different. Compression is observed only when the confining pressure is larger than a certain threshold value. If lower confining pressure is applied, only small volume increases are observed (Josa et al. [15]). It is crucial to understand phenomena, happening during pre-failure stage, accumulation of which is leading to failure (Leroueil [12]).

Cutting slopes is a common practice in transportation projects and as a remediation measure of natural slopes. It is important to understand the deformation patterns that occur not only within the slope itself but also in the excavated area and the crest above, especially if construction in this region is planned. The aim of this study is to investigate the processes taking place during unloading (cutting a slope) followed by a single rainfall event and their combined effect, with stress paths providing valuable insight into these mechanisms. This preliminary study aims to

understand the key processes that will inform the development of further scenarios to investigate the impact of climate on clay slopes.

2. Methods

In this study, a Python-based numerical code FEniCS-Geo was employed. It enables hydro-mechanical coupled analysis, accounts for unsaturated behaviour and incorporates advanced constitutive models. Mathematical formulation of the hydro-mechanical coupling is presented in Appendix. FEniCS-Geo was originally developed by Abed et al. [1], results of further development are presented in Cheng et al. [2] and Muratova et al. [3] . The code was extended to include multi-layered soil profiles and unloading processes.

The Creep-SClay1S model was selected to represent the behaviour of a sensitive natural clay, as it incorporates anisotropy, destructuration, as well as Lode angle and rate dependency. In critical state models, the strength and stiffness parameters are interconnected. The slope of the critical state line M, commonly treated as a strength parameter, also governs the shape and size of the yield surface, which controls the development of strains and the evolution of state variables. Therefore, conventional methods for calculating the safety factor, such as the strength reduction technique, are not directly applicable: reducing M fundamentally changes the behaviour of the model and makes it no longer representative. Therefore, calculation of safety factor is not performed.

The scope of this paper does not include triggering failure but focuses on investigating the climate-induced hydrological impact on clay slope. It explores how different rainfall scenarios influence the evolution of effective stresses, pore pressures, displacements, and state parameters.

2.3 Creep-SClay1s material model

Three surfaces are used for the description of the state of the soil (Fig. 1), Isaksson, 2025 [7].

- The intrinsic compression surface (ICS)
- The current stress surface (CSS)
- The normal consolidation surface (NCS)

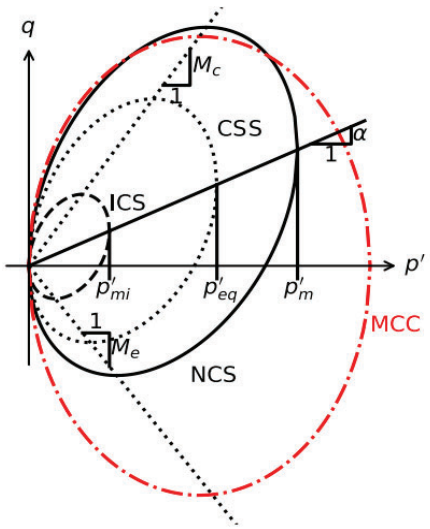

Figure 1. Current state surface (CSS), normal consolidation surface (NCS), and intrinsic compression surface (ICS) of the Creep-SCLAY1S model (Isaksson, 2025 [7])

NCS defines the boundary between the small and large irrecoverable strains. The effect of bonding is incorporated through an imaginary ICS surface, which represents an unbonded soil with the same void ratio and fabric. The CSS represents the current state of effective stresses [8]. These three surfaces have the same shape and orientation but different sizes. They are defined, in the simplified case of the triaxial stress state, by equation:

$$f_{surface} = (q - \alpha p')^2 - (M^2(\theta_\alpha) - \alpha^2)(p'_{surface} - p')p' = 0 \quad (1)$$

where the subscript 'surface' takes the value NCS, ICS, or CSS. The NCS, ICS and CSS size are limited by the isotropic preconsolidation pressure p'_m of the natural clay, the intrinsic isotropic preconsolidation pressure p'_{mi} and the equivalent mean stress p'_{eq}, respectively.

Lode angle formulation is used to enable different values of the critical state stress ratio in triaxial extension M_e and triaxial compression M_c [9] as measured for natural clays:

$$M(\theta_\alpha) = M_c \left(\frac{2m^4}{1 + m^4 + (1 - m^4) \sin 3\theta_\alpha} \right)^{\frac{1}{4}} \quad (2)$$

where $m = \frac{M_e}{M_c}$, θ_α is the modified Lode angle, α is inclination of NCS, ICS and CSS

The total strain rate is expressed by

$$\begin{aligned} \dot{\epsilon_v} &= \dot{\epsilon}_v^e + \dot{\epsilon}_v^c \\ \dot{\epsilon_v} &= \dot{\epsilon}_q^e + \dot{\epsilon}_q^c \end{aligned} \quad (3)$$

The elastic volumetric and deviatoric strain rates are defined by:

$$\begin{aligned} \dot{\epsilon}_v^e &= \frac{\dot{p'}}{K} \\ \dot{\epsilon}_q^e &= \frac{\dot{q}}{3G} \end{aligned} \quad (4)$$

The rate-dependent (creep) strain rates are defined by:

$$\begin{aligned} \dot{\epsilon}_v^c &= \dot{\Lambda} \frac{\partial p'_{eq}}{\partial p'} \\ \dot{\epsilon}_q^c &= \dot{\Lambda} \frac{\partial p'_{eq}}{\partial q} \end{aligned} \quad (5)$$

with a viscoplastic multiplier is defined by:

$$\dot{\Lambda} = \frac{\mu^*_i}{\tau} \left(\frac{1}{OCR^*} \right)^\beta \left(\frac{M_c^2 - \alpha_{K_0^{NC}}^2}{M_c^2 - \eta_{K_0^{NC}}^2} \right) \quad (6)$$

where μ^*_i is modified intrinsic compression index, $\alpha^2_{K_0^{NC}}$ is the inclination of the ICS, CSS and NCS corresponding to that produced by an ID consolidation in normally consolidated state, τ is reference time, β is expressed by:

$$\beta = \frac{\lambda^*_i - \kappa^*}{\mu^*_i} \tag{7}$$

where λ^*_i is modified intrinsic compression index, κ^* is modified swelling index.

The modified over consolidation ratio is defined by:

$$OCR^* = \frac{p'_m}{p'_{eq}} \tag{8}$$

The Creep-SCLAYIS model considers three hardening processes: isotropic hardening, destructuration which affects the size of ICS and NCS, and rotational hardening which affects the orientation of the three surfaces. The isotropic hardening rule relates the change of the intrinsic isotropic preconsolidation pressure p'_{mi} with volumetric creep strains rate as follows:

$$\dot{p}'_{mi} = \frac{p'_{mi}}{\lambda^*_i - \kappa^*} \dot{\epsilon}^c_v \tag{9}$$

The second hardening law is the rotational hardening rule. It relates the evolution of anisotropy to creep strain rates as follows (Sivasithamparam et al. [19]):

$$\dot{\alpha} = \omega \left[\left(\frac{3q}{4p'} - \alpha \right) \langle \dot{\epsilon}^c_v \rangle + \omega_d \left(\frac{3q}{4p'} - \alpha \right) \left| \dot{\epsilon}^c_q \right| \right] \tag{10}$$

The third hardening law relates the degradation of bonding with creep strains. The evolution of structure, characterised by the destructuration rate as a function of the volumetric and deviatoric creep strain rate, is expressed by:

$$\dot{\chi} = -a\chi \left(|\dot{\epsilon}^c_v| - b \left| \dot{\epsilon}^c_q \right| \right) \tag{11}$$

where the absolute rate of destructuration a, and the relative rate of destructuration b, are parameters controlling the rate of destructuration of the soil.

3. Analysis

3.1 The Finite Element model

The slope geometry, mesh, and water table are presented in Figure 2. The model consists of 2 layers: cracked dry crust, marked in brown (first 1.5 meters) and natural clay. Soil parameters are summarised in Table 1.

3.2 Initial conditions

When using advanced constitutive models such as Creep-SCLAY1S, it is crucial to establish accurate initial conditions, as the state parameters of the model significantly influence the results. To achieve this, the unloading process is implemented following the procedure outlined by Brown and Booker [10], consisting of the following steps:

- Gravity loading (elastic stage): A load equivalent to the weight of the excavated soil is applied at the boundary to simulate the initial stress conditions with a horizontal ground surface.
- Constitutive model activation (under gravity loading): The constitutive model is switched to Creep-SCLAY1S while keeping the applied load unchanged.
- Unloading due to excavations/erosion: The load is gradually reduced to zero in increments over time.

Table 1. Parameters of the soil

Parameter	Definition	Value
λ^*_i	Modified intrinsic compression index	0.08
κ^*	Modified swelling index	0.008
υ'	Poisson's ratio	0.2
M_c	Stress ratio at critical state in triaxial compression	1.75
Me	Stress ratio at critical state in triaxial extension	1.2
OCR	Over consolidation ratio	1.2[a]
α_0	Initial value of anisotropy	0.57
ω	Absolute rate of rotational hardening	55
ω_d	Relative rate of rotational hardening due to deviator stress	1.0
ξ	Absolute rate of destructuration	8
ξ_d	Relative rate of destructuration due to deviator stress	0.5
χ_0	Initial amount of bonding	15
μ^*_i	Modified intrinsic creep index	0.0015
τ	Reference time	1.0
e_0	Void ratio	2.0
k_{sat}	Hydraulic conductivity at full saturation, m/d	0.001[b]
a	Parameter of soil-water retention curve	0.1
S_{res}	Residual degree of saturation	0.23
S_{sat}	Degree of saturation at full saturation	1

[a] For dry crust (first 1.5 meters) POP=15 was used.
[a] For dry crust (first 1.5 meters) k_{sat} =0.1 m/d was used to simulate crucks.

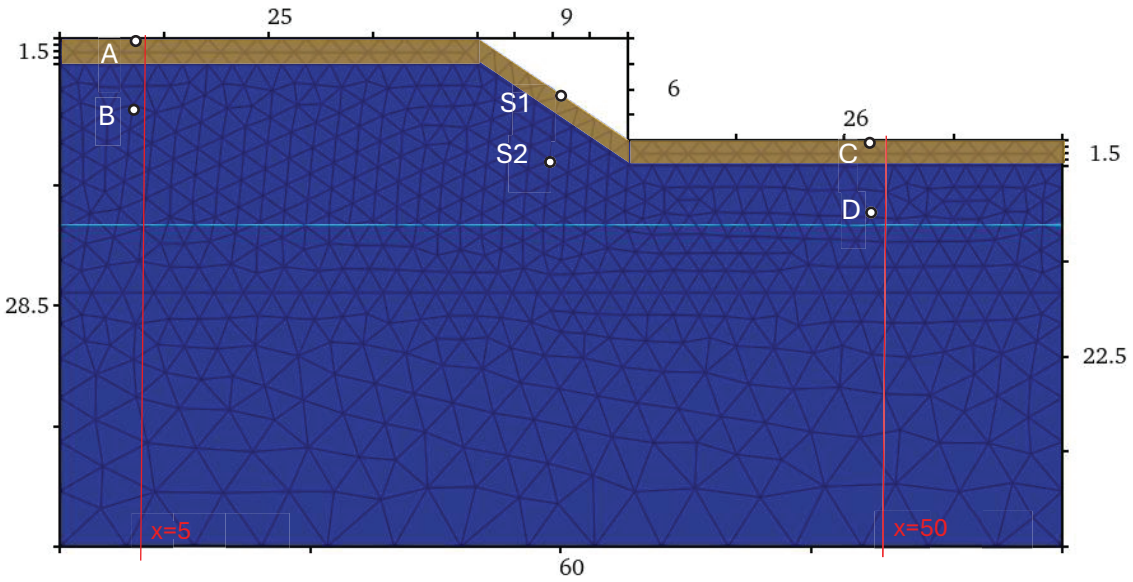

Figure 2. Model geometry, mesh and water level

The slope was cut over a period of 10 days following procedure explained above. A schematic description of the phases is presented on the Figure 3.

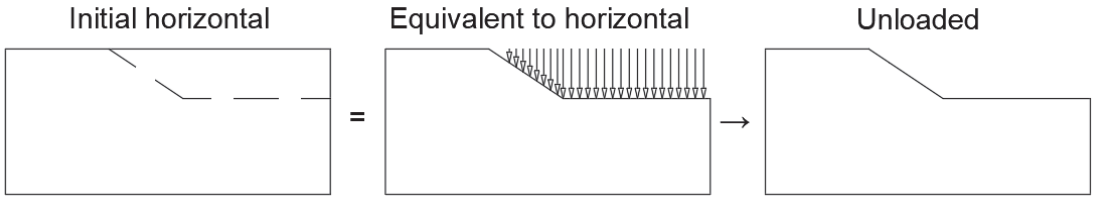

Figure 3. Stages of cutting the slope

Once the excavation is complete, the cut natural clay slope is subjected to different climate scenarios for further analysis.

3.3 Climate scenarios

To analyse the response of different parts of the slope under various climate scenarios, four rainfall intensities were selected to represent seasonal variations throughout the year. Based on statistical data from the Swedish Meteorological and Hydrological Institute (SMHI)[11], the following typical short-term scenarios were identified. In each case, the total volume of infiltrated water remains constant at 300 mm per simulation, ensuring a consistent comparison of the effects of different rainfall intensities.

- Rainfall of 10 mm/day for 30 days
- Rainfall of 15 mm/day for 20 days
- Rainfall of 30 mm/day for 10 days
- Rainfall of 100 mm/day for 3 days – extreme scenario

To summarise, simulations were carried out in the following steps:

- Unloading (cutting the slope) for 10 days; (0-10 day)
- Creep phase (reference rate): The model is allowed to creep for 20 days to establish a reference creep rate; (10-30 day);
- Infiltration phase: Rainfall infiltration is applied:
  - Rainfall of 10 mm/day for 30 days; (30-60 day)
  - Rainfall of 15 mm/day for 20 days; (30-50 day)
  - Rainfall of 30 mm/day for 10 days; (30-40 day)
  - Rainfall of 100 mm/day for 3 days; (30-33 day)
- Post-infiltration creep phase: The model continues to creep for 30 days to analyse the effects of infiltration on slope behaviour during the following month. So depending on rainfall intensity simulation ends at:
  - 90 days for 10 mm/day
  - 80 days for 15 mm/day
  - 70 days for 30 mm/day
  - 63 days for 100 mm/day

4. Results

On the Figure 4 vertical displacements of the points S1 and S2 shown on the Figure 2. The final displacements are results of the combination of the processes happening in the excavated area and crest area. To isolate influence of those processes points A , B, C and D and cross sections near them will be investigated.

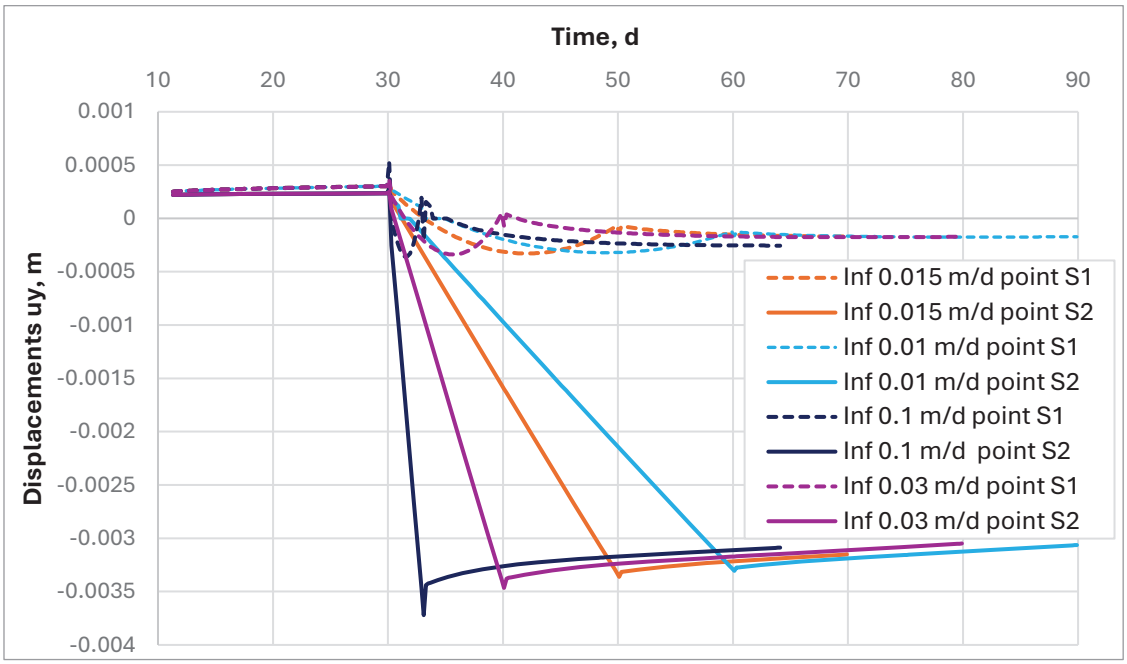

Figure 4. Displacements at points S1 and S2

4.1 Suction and unit weights

The rainfall is influencing the degree of saturation in the affected zone, which is leading to an increase in the unit weight of the soil in accordance with formula [6]. The predicted unit weight profiles (vertical cross-sections at x = 5 and x = 50) at day 0, 33 and 63 are presented in Figure 5.

The predicted suction profiles (vertical cross-sections at x = 5 and x = 50) are presented in Figure 6. Figure 6a illustrates the initial distribution of suction and its evolution at t = 33 days, marking the end of the extreme scenario. Figures 6b and 6c depict the suction profiles for partially saturated zone at 40 and 60 days, respectively. Figure 6d presents the suction distribution at the end of each stage.

The results show that, in all cases, the suction in the upper part of the slope decreases by approximately 60 kPa, reaching a minimum of 32–38 kPa by the end of the infiltration phase. Initially, the zone affected by infiltration extends to a depth of around 3 meters. However, as infiltration progresses, this zone deepens, reaching approximately 5 meters by the end of the post-infiltration creep phase. During the post-infiltration phase, the suction in the upper slope begins to recover toward its initial values, while the suction in the lower portion (from approximately 3 meters deep) gradually decreases.

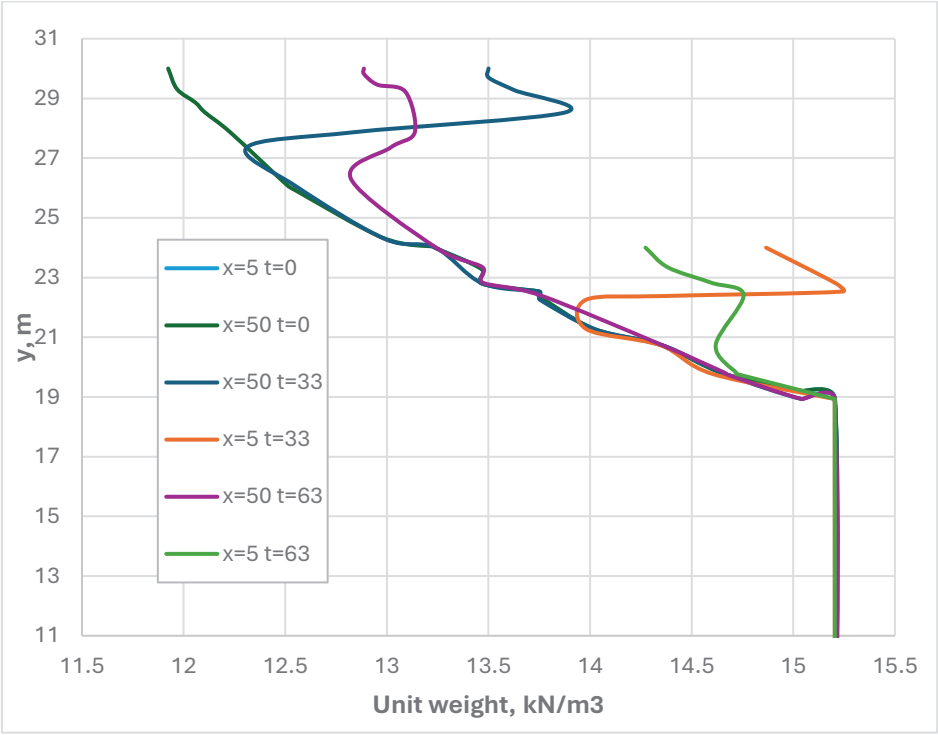

Figure 5. Unit weights profiles

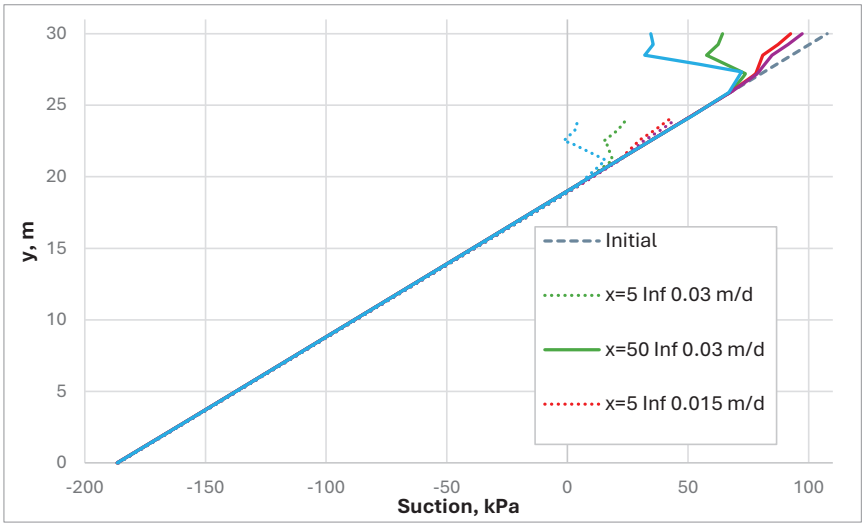

a)

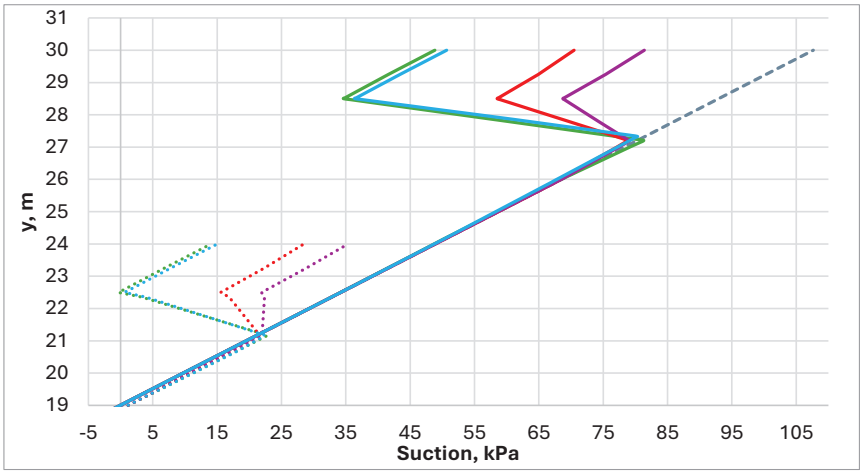

b)

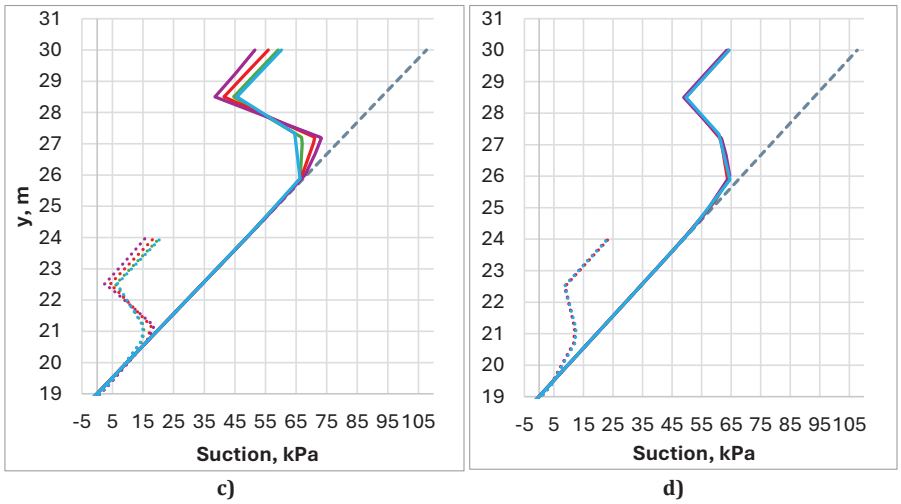

c) d)

Figure 6. Suction cross sections at a) t=33 d b) t=40 d c) t=60 d d) t=end

4.2 Effective stress paths

The changes in the suction and the unit weight of the soil result in variations in the effective stress distribution. The predicted effective stress paths at points A, B, C, and D (see Figure 2) are shown in Figures 7a, 7b, 7c, and 7d, respectively. The normal consolidation surface is marked in black, the intrinsic compression surface is marked in blue, while the initial location of the current stress surface (CSS) is highlighted in red, with points 1 representing the initial stress conditions. During unloading, the effective stresses decrease at points C and D, whereas at points A and B stress paths slide along CSS, which is explained by increase in horizontal stresses. The new stress points at the end of unloading are represented by points 2.

A noticeable difference in OCR*, defined by Equation 8, is observed: in the unloading zone (points C and D), OCR* reaches 3.5 and 2.5, respectively. In contrast, at points A and B, OCR remains nearly unchanged. During infiltration stage at surface points A and C, effective stresses continue decreasing due to a decrease in suction. Conversely, at points B and D, the effective stresses increase. This area is not significantly affected by the reduction in suction; instead, the increase in soil unit weight above these points contributes to the predicted effective stress increase. The position of a stress points at the end of infiltration phase is represented by points 3.

Following the infiltration event, as pore water pressures begin to redistribute, effective stresses at points A and C gradually recover toward their pre-infiltration levels. The updated stress states are marked by points 4. In contrast, points B and D show no significant change in effective stresses during the post-infiltration phase.

These processes occur with the same overall magnitude across all four infiltration scenarios; however, the rate of change differs. For instance, the current stress surfaces (CSSs) evolve at different rates, meaning their size and shape adjustments vary over time. This, in turn, leads to differences in strain and displacement development.

4.3 Vertical displacements

The predicted vertical displacement over time at points A, B, C and D are presented in Figures 8a-8c. Point A is located in a zone that is almost unaffected by unloading, with a low overconsolidation ratio (OCR). As a result, the predicted heave remains minimal during the early stages. However, under high infiltration rates, an increase in elastic deformations is observed toward the end of the infiltration stage when suction reaches minimum. Point B behaves as expected for normally consolidated clay, with settlements due to the increase in effective stress caused by unit weight increase during infiltration. Point C is situated in a zone that is overconsolidated resulting from previous unloading (erosion). In contrast to Point A, a higher uplift response is observed during infiltration. This is caused by a reduction in effective stresses leading to heave, typical of overconsolidated soils on the dry side of the critical state line. Point D is also located in an overconsolidated zone, with a higher OCR than Point B. Thus, lower settlements than at point B are predicted.

By comparing the predicted vertical displacements at day 60 between points A and B, we can see that low infiltration rates cause the smallest displacements, while high infiltration rates lead to the largest. This can be explained by different creep rates due to different loading rates and state conditions, but further investigation needs to be performed to make final conclusions.

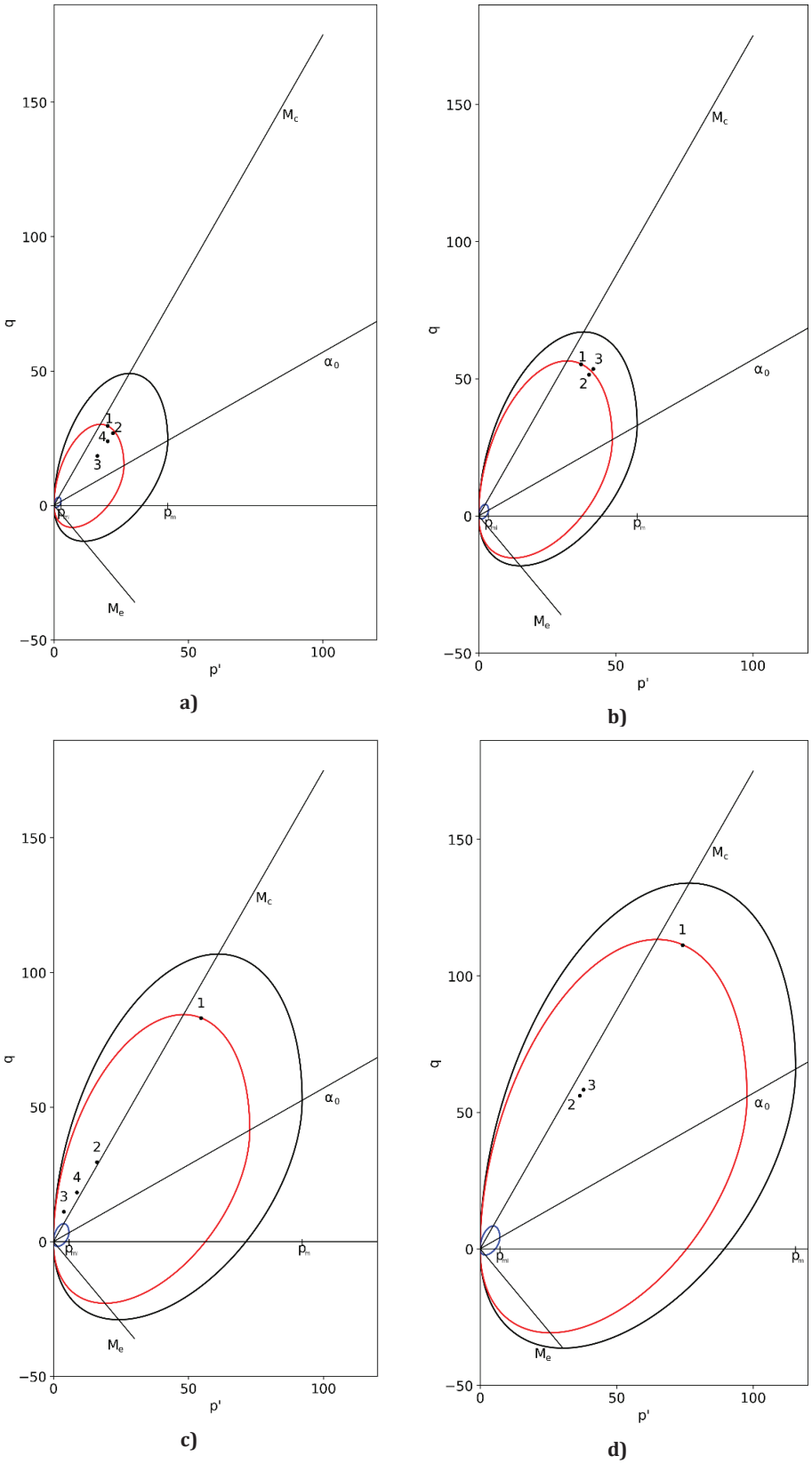

Figure 7. Effective stress paths a) at point A b) at point B c) at point C b) at point D

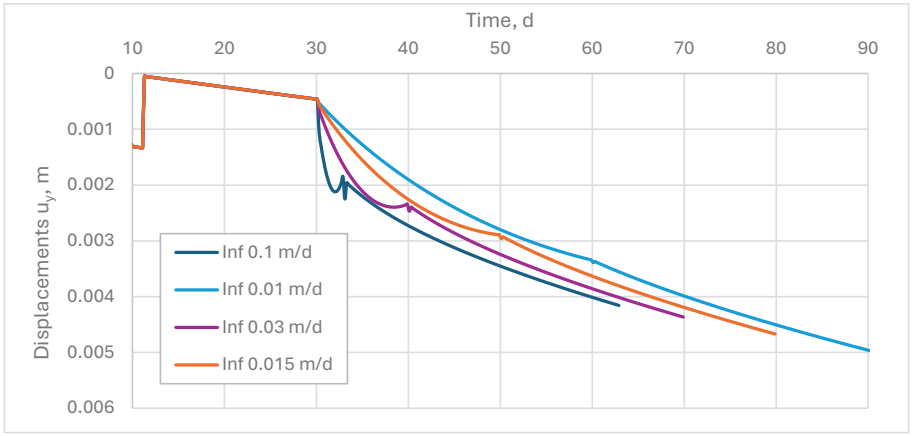

a)

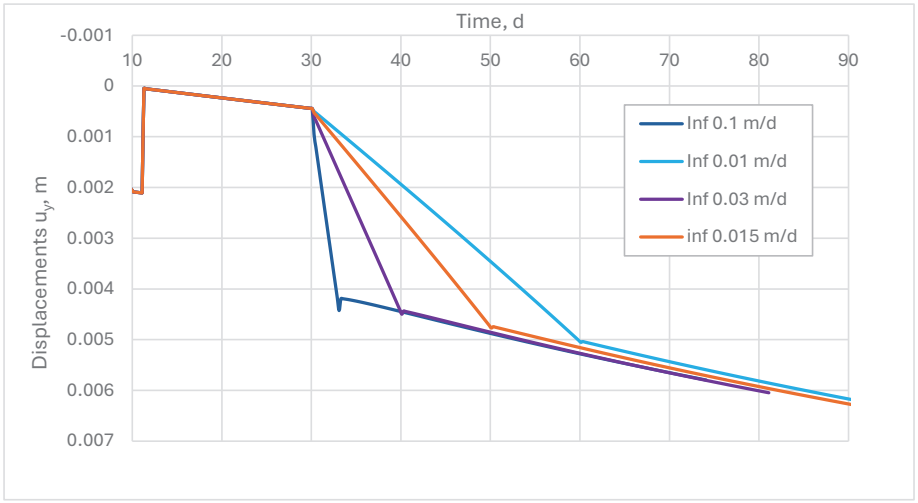

b)

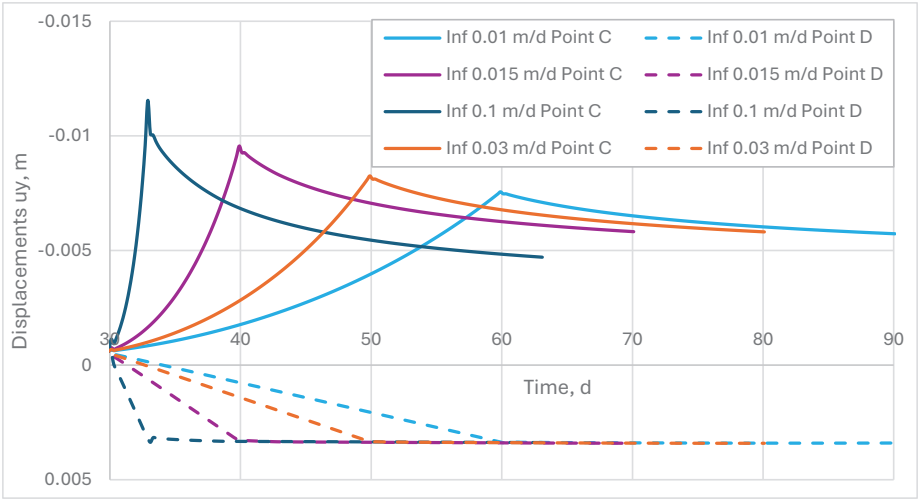

c)

Figure 8. Vertical displacements over time a) at point A b) at point B c) at points C and D

The displacements at point D stay almost the same under all infiltration rates which indicates that deformation is mainly elastic and not affected by time-dependent effects due to the high OCR. Point C shows clear differences in displacement depending on the infiltration rate. Under low infiltration rate, the predicted heave is small and stabilizes early. With medium infiltration, the heave is more noticeable and lasts longer. Under high infiltration rates, the heave is the greatest. This can be explained by the lower permeability of the underlying soil, which becomes even less effective during infiltration. As a result, excess pore pressure cannot dissipate as quickly, leading to a stronger elastic response.

In the area of the slope (points S1 and S2), a combination of two interacting processes is taking place, therefore relatively small displacements are observed in the point S1. It is essential to continue investigating these processes, along with the evolution of stresses, displacements, and state parameters over the long term, particularly as the system approaches a failure state.

5. Conclusions

This study investigates the combined influence of a cut slope and rainfall infiltration of different intensities on the evolution of a natural (sensitive) clay slope. The developed numerical model demonstrates its ability to simulate both unloading and hydro-mechanical coupled processes, which are essential for understanding the behaviour of natural clay slopes. The results clearly show that properly representing the unloading process is critical for accurately capturing the mechanical response of the slope. Capturing these interactions enables a more realistic representation of slope evolution under varying loading and environmental conditions. Additionally, the model effectively incorporates the influence of different infiltration rates, revealing noticeable variations in displacements even during isolated, short-duration rainfall events. This underscores the importance of accounting for infiltration effects in slope stability analysis, as the changes in pore water pressure and soil properties can significantly alter deformation patterns.

In this study, a single rainfall event did not induce instability. However, prolonged rainfall that causes a significant reduction in effective stress may lead to instability. Additionally, Figure 6d illustrates that, given the current permeability values and water level, the rainwater has not yet altered the initial water level by the end of the simulation, so changes in pore pressure will continue. Nevertheless, single rainfall has modified the suction profile in the topsoil. The paper demonstrates the capability of the model to simulate this process accurately, ensuring that all intermediate distributions of pore water pressure and their influence on the mechanical behaviour are accounted for.

In the future, multi-year simulations will be conducted incorporating various rainfall scenarios with different levels of infiltration efficiency, considering different initial hydraulic boundary conditions. However model is accounting for influence of unsaturated behaviour via Bishop's stresses, it is recommended in future utilise models such as Barcelona Basic for modelling dry crust for better modelling drying-wetting behaviour of partially saturated zone. These rainfall scenarios will be based on statistical rainfall data from Swedish Meteorological and Hydrological Institute. The proposed approach will support the assessment of the long-term behaviour of natural slopes under different hydro-meteorological conditions and their potential progression towards failure, i.e. creeping to failure.

Acknowledgements

The work is funded by Formas (Research Council for sustainable Development (Grant 2021-02400), Swedish Research Council (VR 2024-04672) and Swedish Transport Administration (Grant 2022/69758) via BIG (Branchsamverkan in grunden). The work is done as part of Digital Twin Cities Centre that is supported by Sweden's Innovation Agency VINNOVA (Grant 2024-03904).

References

[1] A. Abed, E. Gerolymatou, M. Karstunen: FEniCS simulation of a partially saturated slope under varying environmental loads. Proceedings 10th NUMGE, 2023.
[2] X. Cheng , Y. Li, M. Karstunen, J. Dijkstra, A. Abed: Implementation of a new thermo-viscoplastic soil model using FEniCS platform. Proceedings NGM, 2024.
[3] K. Muratova, A. Abed, M. Karstunen: FEniCS simulation of artesian conditions in clay slope. Proceedings NGM, 2024.
[4] A. Gens, M. Sánchez, D. Sheng: On constitutive modelling of unsaturated soils. Acta Geotechnica 1, 137–137, 2006.
[5] R. Srivastava, T.C. Jim Yeh: Analytical solutions for one-dimensional transient infiltration toward the water table in homogeneous and layered soil. Water Resources Research,1991.
[6] A. Abed, W. Sołowski: A study on how to couple thermo-hydro-mechanical behaviour of unsaturated soils: Physical equations, numerical implementation and examples. Computational Geotechnics 92, 132–155, 2017.
[7] J. Isaksson; On quantifying the installation effects of displacement piles in natural clays. PhD thesis, 2025.
K. Muratova, A. Abed, M. Karstunen: FEniCS simulation of artesian conditions in clay slope. Proceedings NGM, 2024.
[8] J.-P. Gras, N. Sivasithamparam, M. Karstunen, J. Dijkstra: Permissible range of model parameters for natural fine-grained materials. Acta Geotechnica, 13(2), 387–398, 2018.
[9] N. Sivasithamparam, M. Karstunen, P. Bonnier: Modelling creep behaviour of anisotropic soft soils. Computers and Geotechnics, 2015.
[10] P.T. Brown, J.R. Booker: Finite element analysis of excavation. Computers and Geotechnics, 1, 207-220, 1985.
[11] Swedish Meteorological and Hydrological Institute: Precipitation. https://www.smhi.se/en/climate/tools-and-inspiration/climate-indicators/precipitation, Retrieved 2025.
[12] S. Leroueil: Natural slopes and cuts: Movement and failure mechanisms. Geotechnique 51.3, 197–243, 2001.
[13] S. L. Gariano, F. Guzzetti: Landslides in a changing climate. Earth-Science Reviews 162, 227–252, 2016.
[14] S. Boyle, K. Karlsrud, Ø. A. Høydal: Pore-pressure response in a marine clay slope in southeast Norway. Canadian Geotechnical Journal, 46(12), 1391–1405, 2009.
[15] A. Josa, E. E. Alonso, A. Lloret, A. Gens: Stress-strain behaviour or partially saturated soils". European conference on soil mechanics and foundation engineering, pp. 561–564, 1987.

Appendix

Mechanical balance equations

Mechanical balance equation is expressed as:

$$\nabla \cdot \boldsymbol{\sigma} + \boldsymbol{b} = 0 \tag{12}$$

where $\nabla \cdot \boldsymbol{\sigma}$ is the divergence of the total stress tensor and $\mathbf{b}$ is a vector containing the body forces.

To account for the effects of unsaturated soil behavior, Bishop's effective stress approach is applied:

$$\boldsymbol{\sigma}' = \boldsymbol{\sigma}'' + \chi \boldsymbol{s} \tag{13}$$

where $\boldsymbol{\sigma''} = \boldsymbol{\sigma} - \boldsymbol{u_a}$ is the net stress, $\boldsymbol{s} = \boldsymbol{u_a} - \boldsymbol{u_w}$ represent the matric suction. The pore air pressure and pore water pressure are denoted as $\boldsymbol{u_a}$ and $\boldsymbol{u_w}$, respectively. It is generally assumed that the pore air pressure remains at atmospheric level with $\boldsymbol{u_a}$ = 0, so $\boldsymbol{s} = -\boldsymbol{u_w}$.

Based on the approach proposed by Gens et al. [4], the code assumes that parameter χ corresponds to the effective degree of saturation S_{eff}, defined as:

$$\chi = S_{eff} = \frac{(S_r - S_{res})}{(S_{sat} - S_{res})} \tag{14}$$

with S_r , S_{sat} and S_{res} represent the current degree of saturation of the clay, the degree of saturation at full saturation (S_{sat} =1 for most practical cases), and the residual degree of saturation, respectively.

Furthermore, the Soil Water Characteristic Curve (SWCC) is required to describe the hydraulic behavior of the unsaturated clay. In this study, a simplified expression for the SWCC by Srivastava and Yeh [5] is adopted:

$$S_r = (S_{sat} - S_{res}) \cdot e^{-\alpha \cdot s} + S_{res} \tag{15}$$

where α is a fitting parameter. The corresponding hydraulic conductivity function is expressed as:

$$K(s) = K_{sat} \cdot e^{-\alpha \cdot s} \tag{16}$$

The unit weight of soil is dependent on the degree of saturation:

$$\gamma = (1 - n)\gamma_s + nS_r\gamma_w \tag{17}$$

where n is the soil porosity, γ_s is the unit weight of solids, and γ_w is the unit weight of pore water.

The weak formulation of the mechanical balance equation and the finite element discretization yield:

$$\int_\Omega \nabla N_b^T \boldsymbol{M} \nabla N_b \delta\hat{u}\, d\Omega + \int_\Omega \chi \nabla N_b^T \boldsymbol{m^T} \nabla N_b\, \delta\widehat{u_w}\, d\Omega - \int_\Omega N_b\, \delta b d\Omega - \int_\Gamma N_b\, \delta\tau d\Gamma = 0 \tag{18}$$

where N_b represent a shape function, $\delta\hat{u}$ is the increment of nodal displacements, $\delta\hat{u}_w$ is the increment of nodal pore water pressure, δb is increment of body forses and δt is the surface traction increment. The symbol $\boldsymbol{m^T}$ is the transpose of the unity vector and M is the material stiffness matrix.

Water mass balance equation

The governing equation for water mass balance in unsaturated soils, as outlined by Abed and Sołowski [6], is formulated as:

$$\nabla^T \left[\frac{K(s)}{\rho_w g} \cdot (\nabla u_w + \rho_w g)\right] + n\left(\frac{\partial S_r}{\partial s} - \frac{S_r}{K_w}\right)\frac{\partial u_w}{\partial t} + S_r \frac{\partial \varepsilon_v}{\partial t} = 0 \tag{19}$$

where n represents the soil porosity, ρ_w is the density of water, g represent the gravity acceleration and K_w is the bulk modulus of water. The term $\frac{\partial \varepsilon_v}{\partial t}$ represnts the volumetric strain rate which couples hydraulic behaviour with the mechanical behaviour.

The weak formulation of the water balance equation and the subsequent finite element discretization yield:

$$\begin{aligned} &-\int_\Omega \nabla N_b^T \frac{K(s)}{\rho_w g} \nabla N_b\, \delta\widehat{u_w}\, d\Omega + \int_\Omega \nabla N_b^T \frac{K(s)}{\rho_w g} \rho_w g d\Omega \\ &+ \int_\Omega \nabla N_b^T n\left(\frac{\partial S_r}{\partial s} - \frac{S_r}{K_w}\right)\frac{\partial \widehat{u_w}}{\partial t} d\Omega + \int_\Omega N_b\, S_r \frac{\partial \varepsilon_v}{\partial t} d\Omega = 0 \end{aligned} \tag{20}$$